Journal of Oceanography, Vol. 62, pp. 617 to 638, 2006

Thermal and Haline Fronts in the Yellow/East China Seas: Surface and Subsurface Seasonality Comparison

SUNGHYEA PARK* and PETER C. CHU

Naval Ocean Analysis and Prediction Laboratory, Department of Oceanography, Naval Postgraduate School, Monterey, CA 93943, U.S.A.

(Received 24 November 2005; in revised form 24 March 2006; accepted 26 April 2006)

Seasonal variability of surface and subsurface thermal/haline fronts in the Yellow/East China Seas (YES) has been investigated using three-dimensional monthly-mean temperature and salinity data from U.S. Navy's Generalized Digital Environmental Model (Version 3.0). The density-compensated Cheju-Yangtze Thermal/Haline Front has (northern and southern) double-tongues. The northern tongue is most evident throughout the depth from December to April. The southern tongue is persistent at the subsurface with conspicuous haline fronts. The thermal (haline) frontal intensity of the northern tongue is controlled mainly by the temperature (salinity) variation on the shoreward (seaward) side of the front. The cold water over the Yangtze Bank is influential in generating the southern tongue and intensifying the Tsushima Thermal Front. The year-round Cheju-Tsushima Thermal Front is evident throughout the depth and intensifies from July to December. The northern arc of the Yangtze Ring Haline Front is manifest in spring and is sustained until summer, whereas the southern one is fully developed in summer because of eastward migration of the Yangtze Diluted Water. The area showing strong frontal intensity in the Chinese Coastal Haline Front shifts seasonally north and south along the Zhejiang-Fujian coast. The Generation and evolution of YES fronts are closely associated with YES circulation (inferred from the linkage of the water masses). Moreover, the subsurface temperature/salinity evolution on the fronts in the Yellow Sea differs from that in the East China Sea owing to local factors such as wintertime vertical mixing and a summertime strong thermocline above the Yellow Sea Bottom Cold Water.

Keywords:
· Yellow and East China Seas,
· thermal and haline fronts,
· three-dimensional climatology,
· Generalized Digital Environmental Model.

1. Introduction

The Yellow/East China Seas (YES) are bounded by China, Korea, and Japan (Fig. 1). The shelf region, shallower than 200 m, occupies more than 70% of the entire YES (Ichikawa and Beardsley, 2002). Geographical characteristics, Kuroshio intrusion, and river discharge generate thermal and haline fronts: the Kuroshio front that is the transition between the cold East China Sea (ECS) shelf water and the warm Kuroshio water (Qui *et al*., 1990; Oka and Kawabe, 1998; Ivanov *et al*., 2004; Chu *et al*., 2005), the haline front off the Yangtze River mouth where the low salinity water from the river meets high salinity water in the sea (Beardsley *et al*., 1983; Lie *et al*., 2003; Lee *et al*., 2004), and the tidal fronts where cold water suspended by bottom tidal mixing is visible against adjacent water (Lie, 1989; Hao *et al*., 2003; Liu *et al*., 2003). The tidal fronts, which significantly affect the biological productivities, are often coincident with the thermal fronts in YES (Zhao, 1987). These fronts have been identified using in situ or satellite data. For convenience, a surface front here means a front that is detected at the sea surface, whereas a subsurface front occurs below the sea surface.

Satellite data usually have high horizontal resolution and long temporal coverage. Satellite data can be used to identify surface fronts and their long-term features (Hickox *et al*., 2000; Park *et al*., 2004), but not subsurface fronts. In situ observational data can be used to identify surface and subsurface fronts only for short-term variability (much less than a year) in a limited region, but not for year-round variability in a wide region such as YES. Thus, year-round features have not been examined simultaneously for the surface fronts and the subsurface fronts in YES. Since both Yellow Sea (YS) and East China Sea

* Corresponding author. E-mail: spark@nps.edu

(ECS) are in the Kuroshio and monsoon-forcing regimes, the fronts in the two seas are related in terms of frontogenesis, characteristics, and frontolysis. Therefore, large-scale, long-term (T, S) data, such as the U.S. Navy's Generalized Digital Environmental Model (GDEM) data, should be used to identify three-dimensional year-round features of the thermal and haline fronts in YES. In this study, GDEM is used (1) to identify three-dimensional monthly climatology of the fronts, (2) to compare seasonal variability between surface and subsurface fronts, (3) to analyze water mass characteristics across the fronts, frontal intensity, and temperature/salinity evolution on seaward/shoreward side of the fronts, and (4) to explore dynamic relationships among the fronts. To avoid ambiguity, "the climatology of the fronts" is defined as the fronts derived from the climatological data such as GDEM.

2. GDEM

2.1 General description

GDEM has been widely used by the academic community as well as the U.S. Navy since its public release. GDEM-Version 3.0 is a global monthly-mean three-dimensional temperature and salinity dataset with a horizontal resolution of 1/4° over the world oceans with 78 depth levels (unit: m): 0, 2, 4, 6, 8, 10, 15, 20, 25, 30, 35, 40, 45, 50, 55, 60, 65, 70, 75, 80, 85, 90, 95, 100, 110, 120, 130, 140, 150, 160, 170, 180, 190, 200, 220, 240, 260, 280, 300, 350, 400, 500, 600, 700, 800, 900, 1000, 1100, 1200, 1300, 1400, 1500, 1600, 1800, 2000, 2200, 2400, 2600, 2800, 3000, 3200, 3400, 3600, 3800, 4000, 4200, 4400, 4600, 4800, 5000, 5200, 5400, 5600, 5800, 6000, 6200, 6400, 6600. This dataset was built on the U.S. Navy's Master Oceanographic Observation Data Set (MOODS) with 8 million profiles (https://www.navo.navy.mil/ops.htm).

Although the earlier GDEM-Version 2.6 has a 1/6° resolution in YES, two factors hinder us from using it: (1) unrealistic horizontal (T, S) distributions in certain regions, and (2) only four-season data, not monthly data available at deeper depths. The first factor is due to the mix of data collected from different observations. GDEM-Version 3.0 completely replaces GDEM-Version 2.6 using new techniques including newly-derived interpolation schemes, zero-gradient boundary conditions along land boundaries at each depth, and vertical gradient correction. These new techniques effectively eliminate large errors in vertical gradients near the bottom, which often occur in the climatological data.

2.2 Comparison with other climatological data

The climatological datasets have been constructed from different data sources using a variety of techniques.

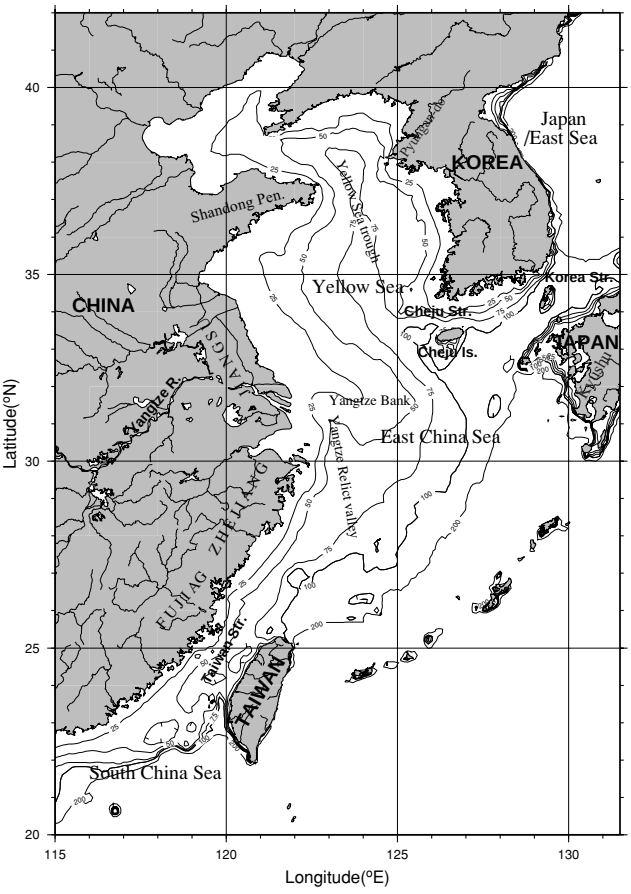

Fig. 1. Geography and bathymetry of the Yellow/East China Seas (YES). Branch-like curves on the land represent rivers. Isobaths of deeper than 200 m are not presented.

No matter how different the datasets, major hydrographic features in a given region should be generally the same among these datasets. It is therefore necessary to examine whether or not GDEM generally exhibits the same hydrographic features in YES compared with other climatological datasets such as the China Marine Atlas (CMA; China Ocean Press, 1992).

In February, distributions of sea surface temperature/salinity are quite similar between GDEM and CMA except for the isothermals/isohalines that connect the Cheju Strait to the Yangtze River mouth and then extend more southward along the Zhejiang-Fujian coast in CMA (Figs. 2, 6 and 8). The discrepancy might be caused by the lack of observational data near the Chinese coast in GDEM. In May and August, cold cores along the Korean coast are stronger in CMA than in GDEM. At 50 m depth the two datasets are in good agreement in term of location and variability of cold water in the central YS and location and seasonal migration of 34.0 psu isohaline in May, August, and November. At the surface the two datasets

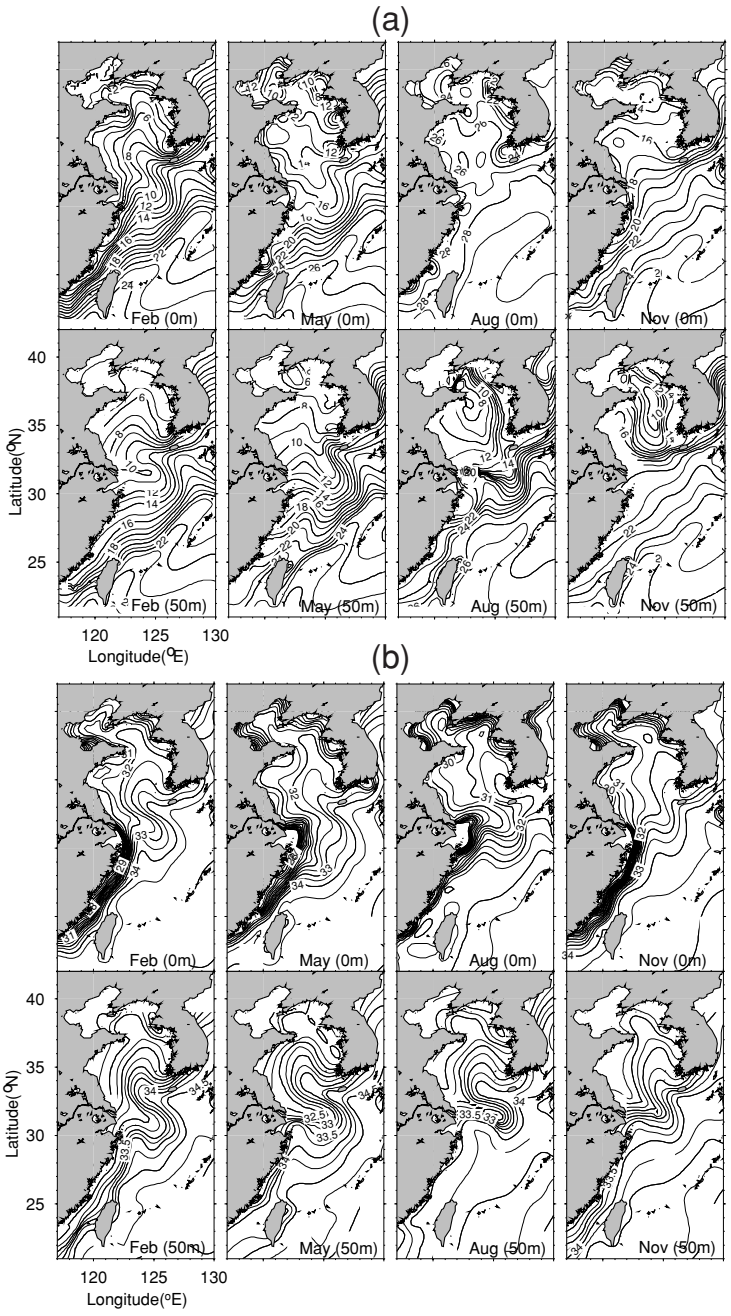

Fig. 2. China Marine Atlas: horizontal distributions of temperature (a) and salinity (b) at 0 and 50 m depths. Isohalines of lower than 26 psu are omitted.

are in discrepancy in salinity distribution in May and August. The Yangtze River plume has a strong salinity gradient near the low-salinity core (close to the coast) and a weak gradient away from the core in CMA, but such a feature is not shown in GDEM (the salinity field is excessively smoothed). The core is shifted seaward in GDEM. Moreover, the horizontal interpolation technique that is good for global climatology may not be satisfactory for the frontal features. Nevertheless, both datasets show common features such as: (1) the Yangtze River plume extending north and south in May but east in August, and (2) appearance and disappearance of the low salinity water from the Yangtze River mouth to the Taiwan Strait. The two datasets are therefore generally in agreement.

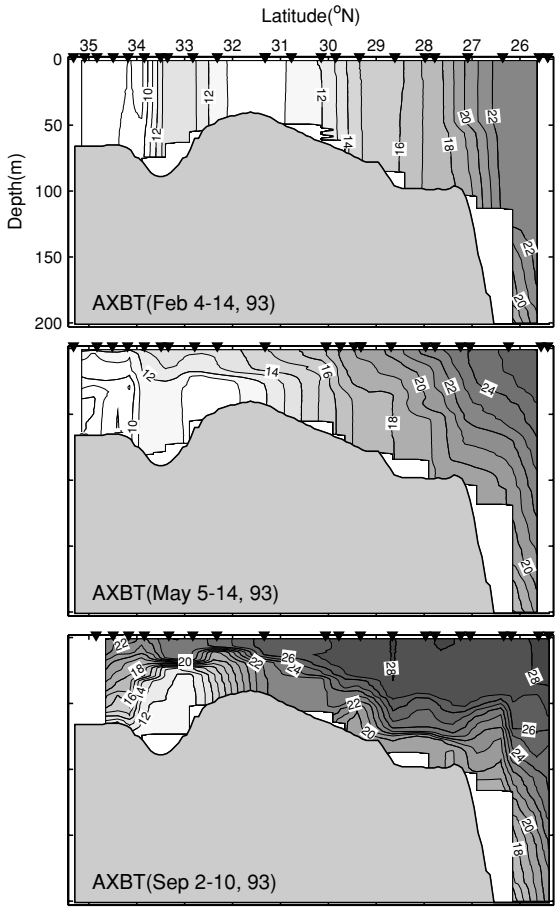

Fig. 3. Vertical temperature cross-section along 125°E from the AXBT observations on February 4–14 1993, May 5–14 1993, and September 2–10 1993. Downward pointing triangles indicate stations of AXBT deployment.

2.3 Comparison with in-situ observations

Any climatological dataset including GDEM has inevitable weakness in detecting fronts. This weakness arises because the climatological dataset smoothes out the fine features of temperature and salinity profiles such as intrusion, interleaving, and inversion, weakens frontal intensity, and blurs a sharp frontal zone. Before identification of the climatology of fronts from GDEM, similarity and dissimilarity in the fronts in YES are analyzed comparatively between GDEM (Fig. 9) and three in-situ observations using the airborne expendable bathythermograph (AXBT) during February 4–14 1993, May 5–14 1993, and September 2–10 1993 (Furey and Bower, 2005; Fig. 3).

In February, the vertical temperature distributions along 125°E are quite similar in frontal location and strength between the two datasets (Figs. 3 and 9): 10–12°C on 33.5–34.0°N, 13–15°C on ~30°N, and 18–22°C on ~27°N. The Kuroshio front on the ECS shelf break (~27°N) shows seasonal variability at the upper 100 m depth. In May the southern part of the cold water (16–17°C) reaches 30°N and forms a front at the subsurface. In September, a strong horizontal gradient forms between the cold water (<12°C) in YS and the warm water (~32°N) in ESC. Subsurface water (<22°C) intrudes into the ECS shelf and the thermocline follows the bottom topography of the shelf. On the other hand, fine features are detected only in the AXBT data, such as an extremely strong thermocline on the top of the cold water, a bundle of isotherms following the bottom topography in September, sharp boundary of fronts, and thermocline intrusions and step-like structures near fronts. These fine structures around fronts will not be discussed in this paper.

YES occasionally experiences short-term episodic variability, such as weekly and semiweekly responses of sea surface height to the wind, intermittent intrusion of warm saline water into YS through collapse of a front around Cheju Island in winter, and migration of the patch-shaped Yangtze Diluted Water (Jacobs *et al*., 1998; Lie *et al*., 2001). These events certainly affect the fronts, and consequently make the synoptic fronts different from their monthly climatology. However, overall features of the synoptic fronts still resemble those of the fronts from the climatological data. The fronts from the climatological data are dynamically associated with climatological circulation of YES, as exhibited in the distributions of fronts from the two datasets. It is therefore feasible to detect the fronts from the climatological data, GDEM, to analyze their seasonality, and to explore dynamic relationship among the fronts.

3. Spatial and Seasonal Variability of Fronts

3.1 Detection of front

Let $\psi(i, t)$ be a variable (temperature or salinity in this study) with (i, t) the spatial and temporal indices. The monthly horizontal temperature and salinity gradients are calculated on each data point

$$|\Delta\psi(i,t)| = \sqrt{\left(\frac{\partial\psi(i,t)}{\partial x}\right)^2 + \left(\frac{\partial\psi(i,t)}{\partial y}\right)^2}, \qquad (1)$$

at 0 (the sea surface), 25, 50, and 75 m depths to detect the fronts. Several criteria have been used to identify thermal fronts: 1–1.4°C/100 km for mild fronts such as in the central South China Sea (Chu and Wang, 2003) and 3°C/100 km for strong fronts such as in the Japan/East Sea*

*The Editor-in-Chief does not recommend the usage of the term "East Sea" in place of "Japan Sea".

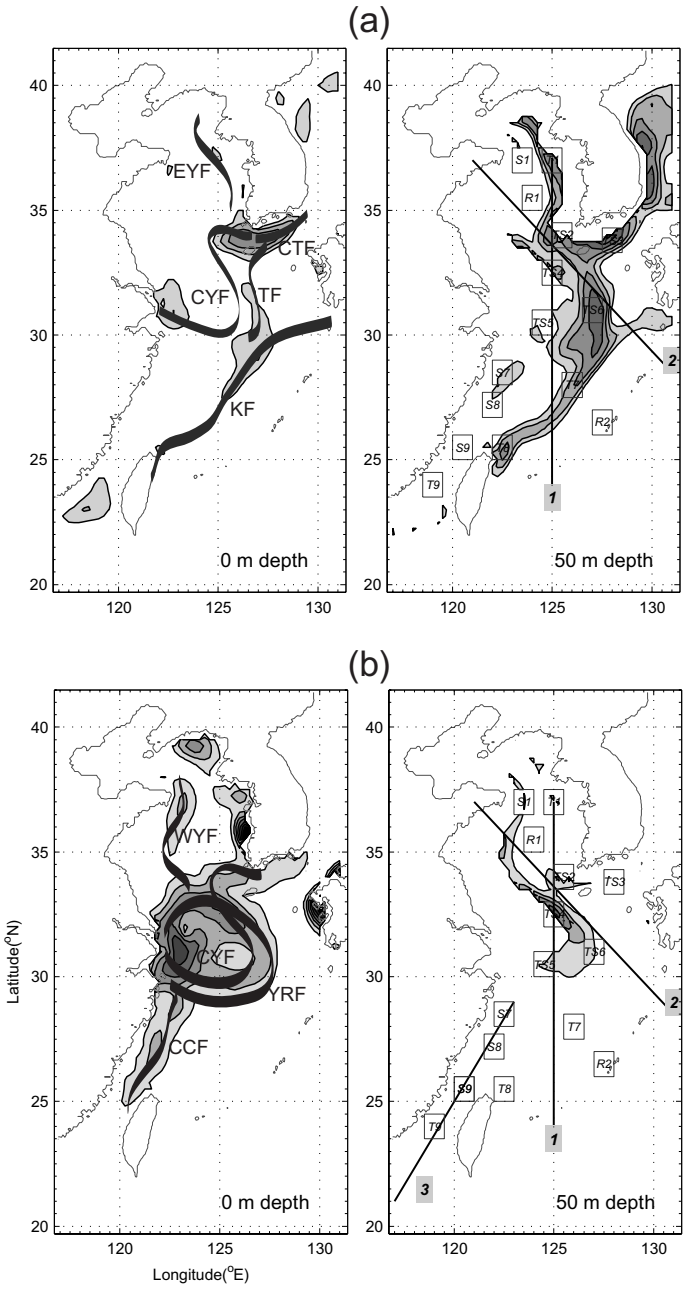

Fig. 4. Location of (a) thermal fronts: Kuroshio Front (KF), Cheju-Yangtze Front (CYF), Cheju-Tsushima Front (CTF), Tsushima Front (TF), and eastern Yellow Sea Front (EYF) and (b) haline fronts: Cheju-Yangtze Front (CYF), Yangtze Ring Front (YRF), Chinese Coastal Front (CCF), and western Yellow Sea Front (WYF). Background is distribution of annual-mean temperature (salinity) gradient. Regions where temperature (salinity) gradient is higher than 2°C/100 km (0.5 psu/100 km) are shaded with a contour interval of 1°C/100 km (0.25 psu/100 km).

(Park *et al.*, 2004). A criterion of 2°C/100 km is selected to identify the thermal fronts in YES, because they are weaker than those in the Japan/East Sea and stronger than those in the South China Sea. Similarly, the haline fronts are identified by the salinity gradient higher than 0.5 psu/100 km (Fig. 4).

Using these criteria (2°C/100 km, 0.5 psu/100 km), a strong thermal front is identified but no haline front is detected along the ECS continental shelf. This is caused by the coarse GDEM resolution (1/4°) since the width of haline fronts (~20 km) is much narrower than the width of thermal fronts (>50 km) in the in-situ data (Lee *et al.*,

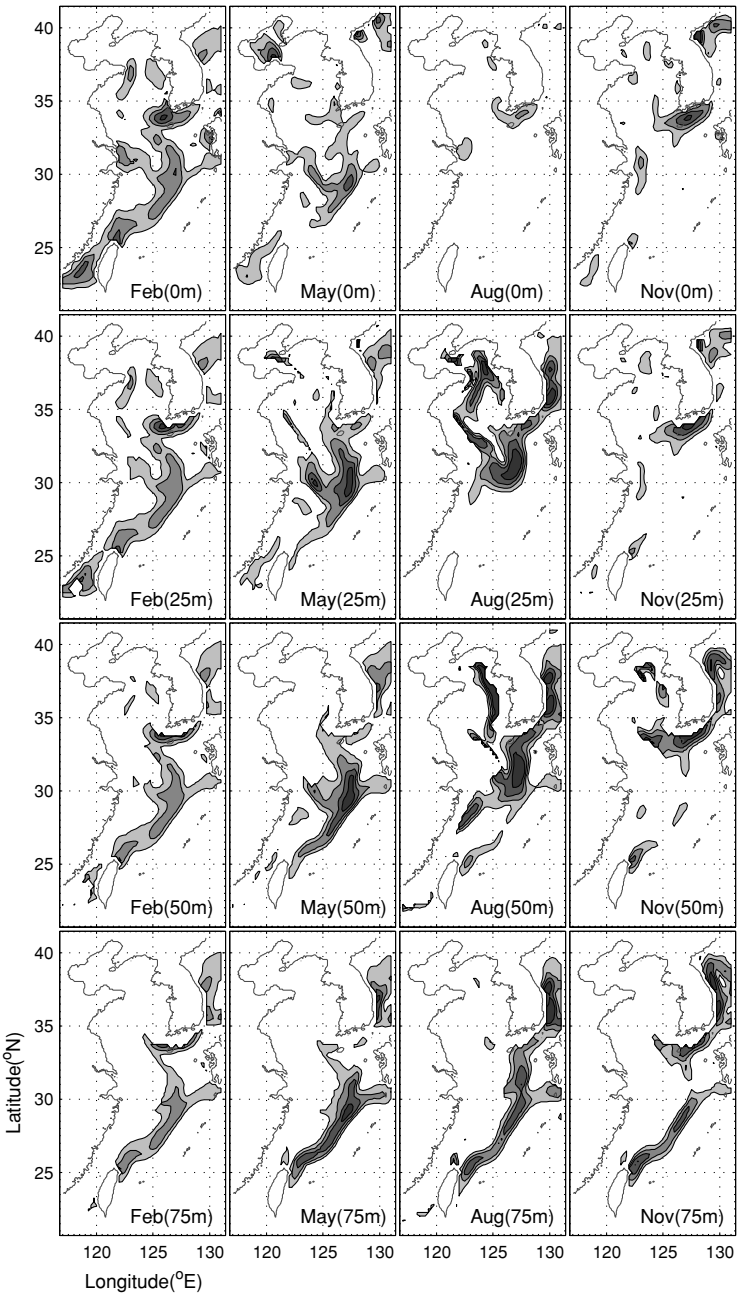

Fig. 5. Horizontal distributions of thermal fronts at 0, 25, 50, and 75 m depths in February, May, August, and November. Regions where temperature gradient is higher than 2°C/100 km are shaded with a contour interval of 1°C/100 km.

2003). Shallow shelf (depth < 50 m) thermal fronts near the Jiangsu-Zhejiang-Fujian and the Pyungan-do coasts are detected using the satellite sea surface temperature data (Hickox *et al*., 2000), but not in GDEM. Furthermore, raw profiles to build GDEM are less frequently observed in salinity than in temperature and on such shelves than in the open ocean. It is understandable that the low salinity plume along Zhejiang coast in February detected from CMA is not seen in GDEM (Fig. 2).

Five major thermal fronts and four major haline fronts are detected in YES using GDEM (Fig. 4). The thermal fronts are the Kuroshio Front (KF), Cheju-Yangtze Front (CYF), Cheju-Tsushima Front (CTF), Tsushima Front (TF), and eastern Yellow Sea Front (EYF). The haline fronts are Cheju-Yangtze Front (CYF; salinity-CYF resembles temperature-CYF in horizontal location and

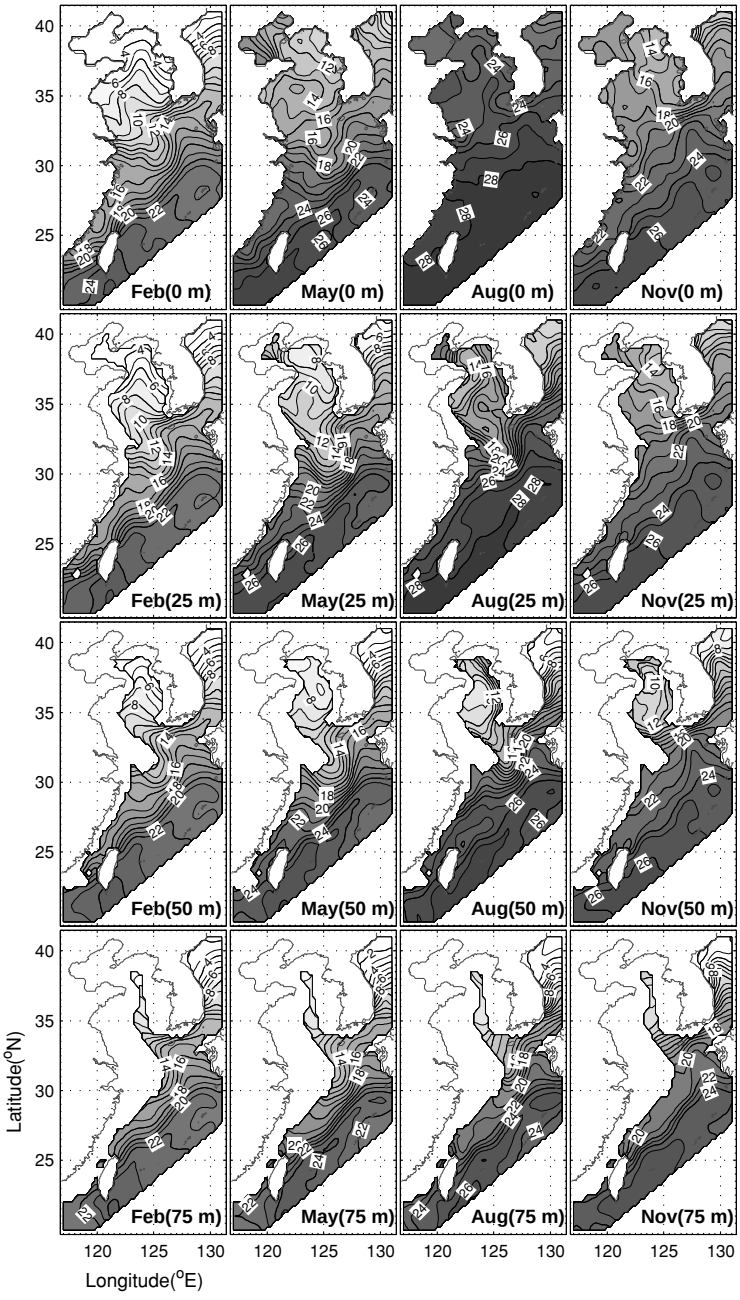

Fig. 6. Horizontal distributions of temperature at 0, 25, 50, and 75 m depths in February, May, August, and November.

shape, and it will be named "thermal CYF" or "haline CYF" when needed to avoid confusion), Yangtze Ring Front (YRF), Chinese Coastal Front (CCF), and western Yellow Sea Front (WYF). Their locations agree with those in synoptic and satellite observations (Ning *et al*., 1998; Hickox *et al*., 2000; Lie *et al*., 2000, 2003; Son *et al*., 2003). This agreement demonstrates that GDEM is valid in detecting the fronts in YES.

3.2 Surface thermal fronts

In this study February, May, August, and November represent winter, spring, summer, and fall, respectively. Most thermal fronts are manifest in winter (Fig. 5). Sea surface temperature on the shelf is strongly affected by the bottom depth, because the thermal inertia of a water column on the shelf is linearly proportional to the bottom depth (Xie *et al*., 2002). As a result the distributions of

wintertime surface thermal fronts and surface temperature seem to mirror the bottom topography (Figs. 5 and 6). Here, CYF is represented by slant-S (double-tongue)-shaped isotherms connecting Cheju Island and the Yangtze River mouth with a northern tongue in the east and a southern tongue in the west. The warm (>12°C) northern tongue of CYF is in the YS trough (Fig. 9) and is caused by the intrusion of warm water (Seung and Shin, 1996), which is often referred to as the Yellow Sea Warm Current. The cold (<12°C) southern tongue of CYF on the Yangtze Bank (Fig. 9) follows the isobaths of 50–70 m with an intensity of 1–2°C/100 km and is caused by the formation of the wintertime cold water and the southeastward intrusion of the cold water. The southeastward intrusion is often referred to as the southward coastal current along the Shandong peninsula-Jiangsu coast driven by the northerly/northwesterly winter monsoon (Hsueh, 1988; Riedlinger and Jacobs, 2000). KF is a shelf break front extending from sea surface to bottom on the ECS shelf break (isobaths of 100–200 m) between east of Taiwan and Kyushu (Figs. 5, 6, 9 and 10). A weak front is developed in the Taiwan Strait from fall to spring. In winter the Kuroshio water is blocked in the Taiwan Strait due to the bottom topography and northeasterly wind (Jan *et al*., 2002), and therefore this front is generated between the blocked warm Kuroshio water and cold coastal water off Fujian. Southward coastal cold currents along the Korean coast and along the Shandong peninsula-northern Jiangsu coast and the northward Yellow Sea Warm Current along the YS trough forms a convex pattern of the isotherms on the central YS (Hsueh, 1988; Riedlinger and Jacobs, 2000; Jacobs *et al*., 2000). This pattern is consistent with the Shandong Peninsula Front and Kyunggi Bay Front identified by Hickox *et al*. (2000).

In spring the northern tongue of CYF disappears as the flow entering YS weakens. The southern tongue of CYF partly weakens (~1°C/100 km) and shrinks at its western part as the volume transport through the Taiwan Strait increases and the southward coastal current along the Shandong peninsula-Jiangsu coast weakens (Naimie *et al*., 2001). The southern tongue changes direction from southeastward to southward and then joins KF at its southern margin with the temperature gradient of 3°C/100 km.

In summer the strong basin-wide downward heat flux causes the formation of the seasonal thermocline, which follows the bottom topography on the shelf (Figs. 9 and 10). The sea surface temperature is quite uniform, ranging from 23°C to 28°C (Chu *et al*., 1997a, b). As a result all fronts are barely detected.

In fall all the fronts are still weak (Hickox *et al*., 2000), except CTF between Cheju Island and Tsushima Island, with intensity 3–4°C/100 km. This front is caused by convergence of the Tsushima Warm Current with the cold coastal water off the south coast of Korea. After the onset of the winter monsoon, heat escapes faster from ocean to air in the shore than in the sea. A thermal front from sea surface to bottom is formed at the boundary between YS and ECS, around 33°N (Fig. 10). KF reemerges near sea surface above the ECS shelf break.

3.3 Subsurface thermal fronts

EYF is strongest (6°C/100 km) at 50 m depth in summer. The cold region off the west coast of Korea migrates southwestward as it deepens in spring (Fig. 6), spreads out from the surface north of 37°N to the near-bottom in the YS trough (Fig. 9) as the Yellow Sea Bottom Cold Water (YSBCW) is ventilated. CYF shrinks remarkably from spring to summer (Figs. 5 and 6). The northern tongue of CYF disappears at depths deeper than 25 m as the warm water intrusion into YS weakens or disappears (Teague and Jacobs, 2000; Naimie *et al*., 2001), and is substituted by cold water (<12°C) (Fig. 9). However, the southern tongue of CYF is sustained. TF is viewed as a branch of KF, which originates at 127–128°E and 30°N, extends northward, and reaches CTF at its northern tip in spring and summer (Figs. 5 and 6). TF occasionally includes the eastern part of the southern tongue of CYF when the tongue migrates eastward in summer, reaching an intensity of about 5°C/100 km at 50 m depth. CTF occurs all year round but is conspicuous (3–4°C/100 km at 50 m depth) in summer and fall because of the increased volume transport from the Tsushima Warm Current (Perkins *et al*., 2000; Jacobs *et al*., 2001). A minor front, which is associated with the Taiwan Warm Current, is found at 122–124°E and 27–30°N at 25 m and 50 m depths from spring to summer (Fig. 5).

At 75 m depth KF is nearly motionless all year round despite its seasonal change of intensity. Across the front the temperature changes from 17°C to 21°C (gradient of 2–3°C/100 km) in winter and from 21°C to 25°C (gradient of 4°C/100 km) in summer, which agrees well with an analysis of water properties along the PN line (Oka and Kawabe, 1998). KF shows a maximum temperature gradient at a branching location (127–128°E and 30°N) known as one of two preferable locations of the Kuroshio intrusion in ECS, where KF is divided into the northern branch (i.e., TF) and the eastern branch (Huh, 1982; Hsueh, 2000; Tseung *et al*., 2000). The strong temperature gradient at the shoreward boundary of KF in summer is due to the enhanced bifurcation of the Kuroshio from summer to fall (around 25–100 m depth in 31–32°N in Fig. 10). This northern branch can be, at least, one component of the Tsushima Warm Current (Isobe, 1999; Ichikawa and Beardsley, 2002).

At depths deeper than 75 m KF is the most evident and nearly motionless all year round (not shown). In contrast to 75 m depth, both frontal intensity and temperature difference across the front are steady throughout the

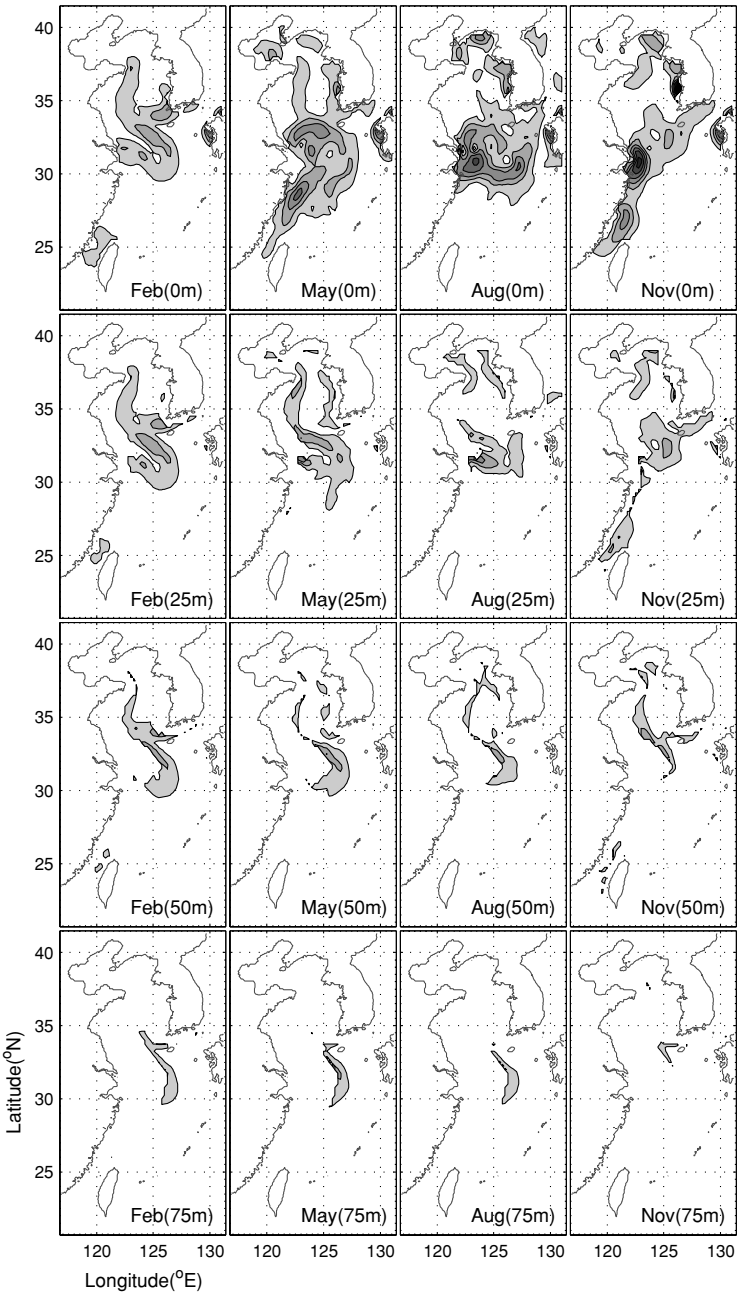

Fig. 7. Horizontal distributions of haline fronts at 0, 25, 50, and 75 m depths in February, May, August, and November. Regions where salinity gradient is higher than 0.5 psu/100 km are shaded with a contour interval of 0.25 psu/100 km.

year; however, the frontal intensity at ~100 m depth is weaker from December to March than in other months, because winter mixed layer often deepens to 150 m depth in winter. CTF and TF are detected at 100 m depth but are weaker than at 75 m depth. Around 200 m depth a front occurs east off Taiwan all year round, which is related to the Kuroshio intrusion into ECS, i.e., one of two preferable locations of the Kuroshio intrusion into ECS. Its frontal intensity increases slightly from April to September.

3.4 Surface haline fronts

In winter salinity distribution resembles temperature distribution in the double-tongue-shaped CYF pattern and the northward convex pattern in the central YS with a weak salinity gradient along the Kuroshio current (Figs.

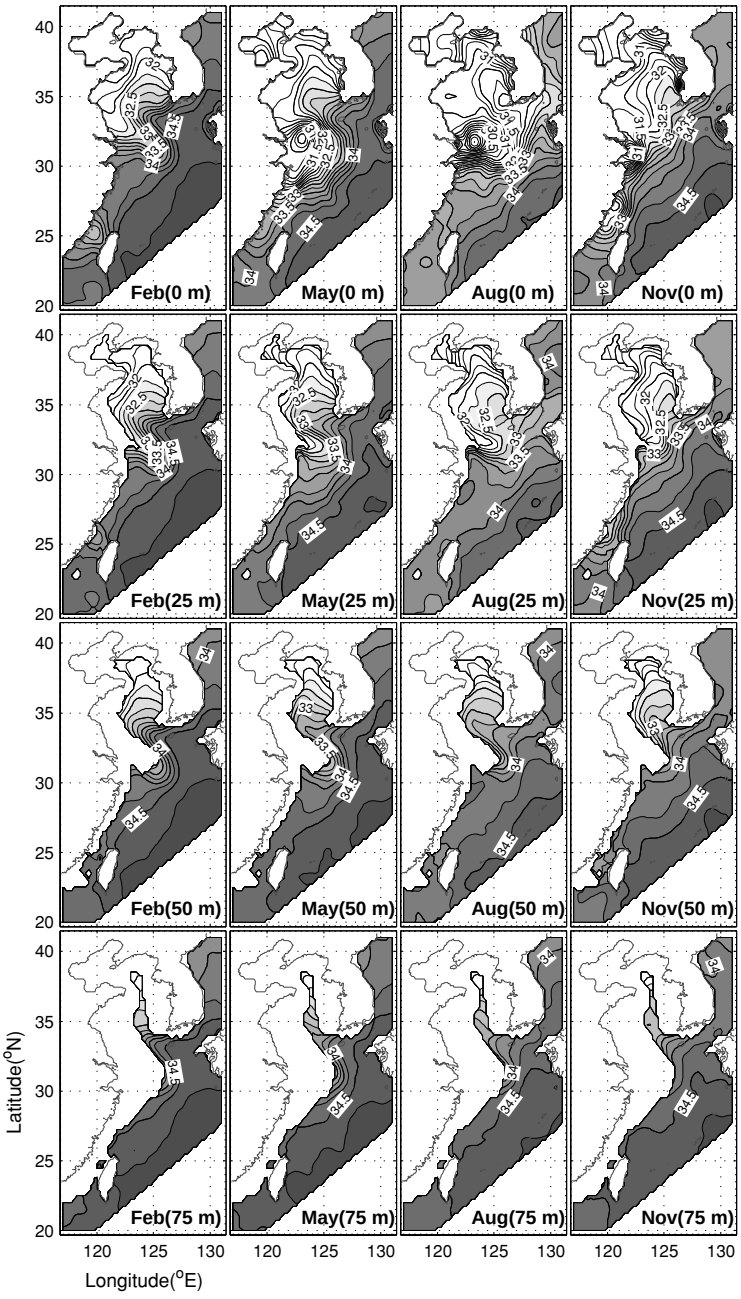

Fig. 8. Horizontal distributions of salinity at 0, 25, 50, and 75 m depths in February, May, August, and November.

7, 8 and 9). WYF appears with intensity ~1 psu/100 km as the saline Yellow Sea Warm Current flows northward against the fresh cold coastal water off Shandong peninsula-northern Jiangsu, which flows southward throughout the depth all year-round, except at the surface in summer (Guan, 1994).

Yangtze River discharge is regarded as an overwhelming freshwater source, which changes the salinity distributions in the southern YS and the northern ECS (Gao *et al*., 1992; Chen *et al*., 1994; Chang and Isobe, 2003). It increases from spring to summer. As the Yangtze River plume moves out of the river mouth, YRF emerges with an intensity of ~2 psu/100 km and a minimum salinity of ~29 psu (in spring). This minimum salinity is higher than that in other datasets (<26 psu in Beardsley *et al*., 1983; China Ocean Press, 1992). The saline northern tongue of CYF and the fresh Yangtze River plume generates the northern arc of YRF. The Yangtze

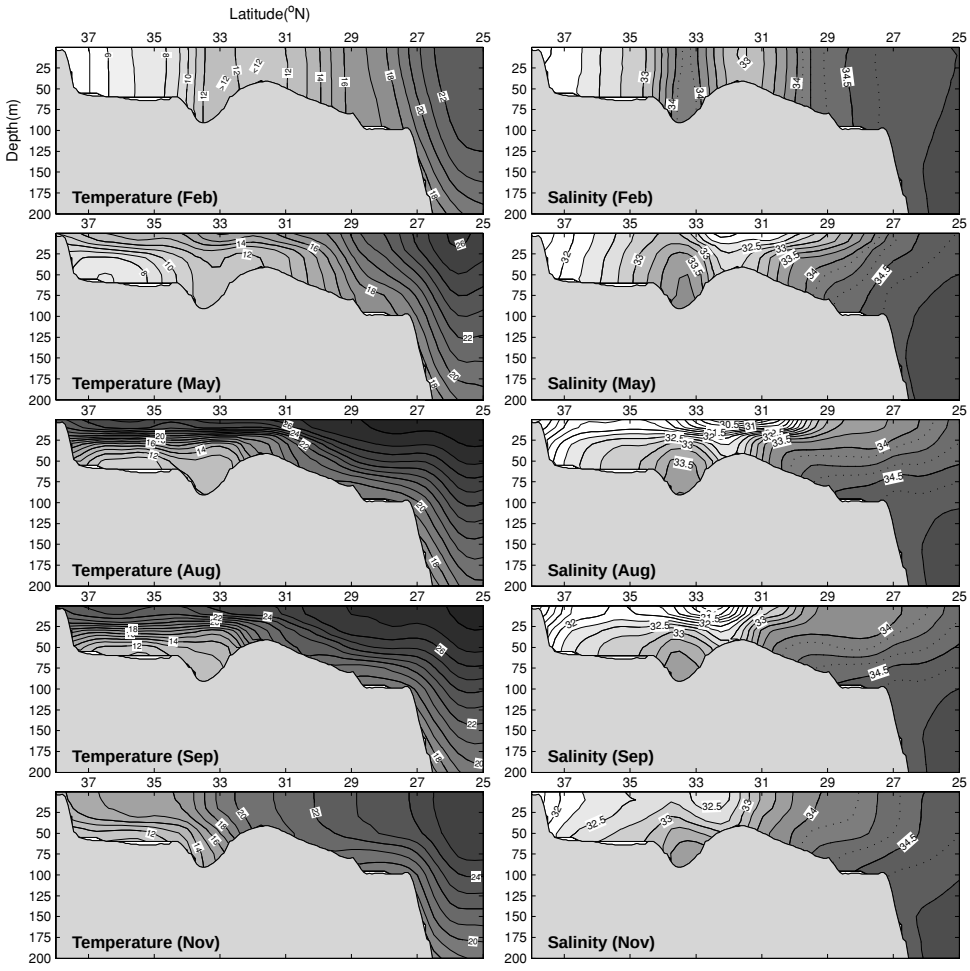

Fig. 9. Vertical temperature and salinity cross-sections along 125°E (a strait line labeled "1" in Fig. 4).

Diluted Water is low salinity water (~32 psu) diluted by the Yangtze River plume. The southern tip of this plume is aligned along the Chinese coast with several nearby minor rivers adding freshwater. Thereby, CCF emerges along the Zhejiang-Fujian coast extending from 25°N to 30°N with an intensity of ~2.5 psu/100 km at 122–123°E and 29°N.

In summer YES is entirely diluted by a maximum river runoff. CYF disappears except around Cheju Island. The well-developed CCF from winter to spring weakens due to the enhanced Taiwan Warm Current and the southerly/southeasterly summer monsoon. The Yangtze Diluted Water extends farther eastward in summer than in spring, because the northerly/northeasterly winter monsoon still affects YES in spring (Lee and Chao, 2003). The low salinity water (<32 psu) moves from the Yangtze River mouth to the Korea Strait (Chang and Isobe, 2003; Lie *et al*., 2003; Lee *et al*., 2004). The intensity of the southern arc of YRF becomes strong (1.5–2 psu/100 km) owing to this eastward/northeastward extension. The vertical salinity cross-section along 125°E (Fig. 9) also shows the northward spread of YRF in 29.5–35°N and a strong salinity gradient in the southern arc in 29–31°N.

In fall the low salinity plume still exists off the Yangtze River mouth because the Yangtze River discharge is higher than the annual-mean from July to mid-October (Chang and Isobe, 2003). It hugs the Zhejiang-Fujian coast as the northeasterly winter monsoon begins, causing the emergence of CCF. The newly discharged Yangtze River water and part of the low salinity water discharged in the preceding summer are distributed in the southern YS and the northern ECS. These waters are transported to the Korea Strait, developing a wide salinity front (1–1.5 psu/100 km) that stretches from off the Yangtze River mouth to the Korea Strait. The monthly-mean of these freshwater transport through the Korea Strait is estimated as 5.6×10^4 m^3s^{-1} from October to December (Chang and Isobe, 2003), which is comparable to the annual-mean Yangtze River discharge of 3.0×10^4 m^3s^{-1}.

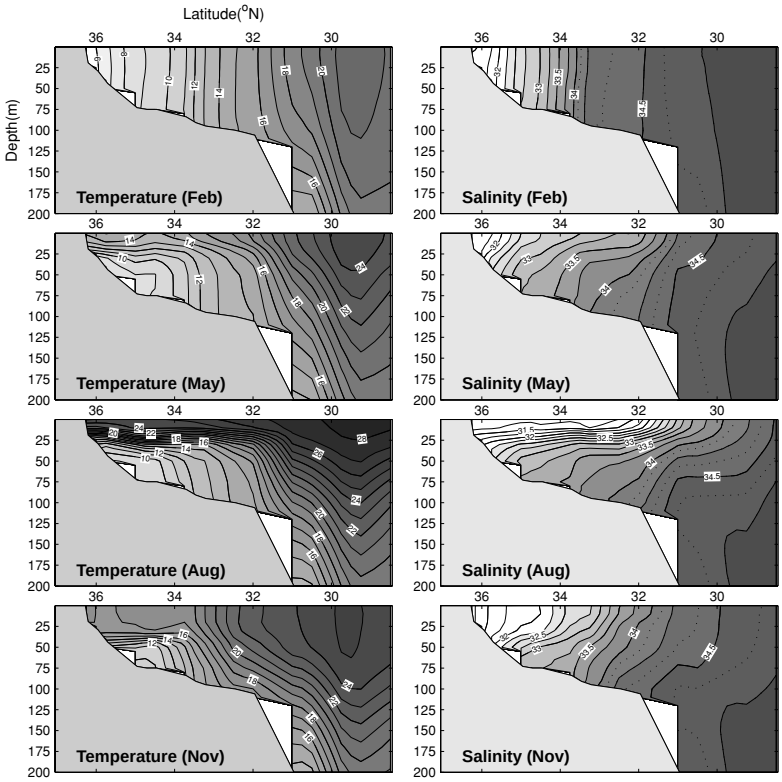

Fig. 10. Vertical temperature and salinity cross-sections across the Yellow Sea trough and the East China Sea shelf (a strait line labeled "2" in Fig. 4).

3.5 Subsurface haline front

The Yangtze River plume is seldom detected at the subsurface because it appears at depths shallower than 15 m (Beardsley *et al*., 1983; Chang and Isobe, 2003; Lie *et al*., 2003). Instead, CYF and WYF are dominant at the subsurface. The northern tongue of CYF, high salinity water (>33.5 psu) in the YS trough, is most evident in winter and least evident in summer (Figs. 7, 8 and 9). This tongue is caused by the northwestward advection of saline water, which persists all year round according to the salinity distribution at 50 m depth (Lie *et al*., 2001). Isohalines stay inclined shoreward near the bottom from spring to fall (for density compensation), even when isotherms are inclined seaward near bottom (Fig. 10). The southern tongue of haline CYF, low salinity water (<33.25 psu) on the Yangtze Bank, is detected at the subsurface all year round (Fig. 9). It is caused by a continuous supply of freshwater from the Shandong peninsula-Jiangsu coast and saline water from the southern ECS, i.e., the Kuroshio water that intrudes northward at the Yangtze Relict River valley by development of bottom friction layer (Jacobs *et al*., 2000).

At depths deeper than 75 m the salinity gradient is high along the Kuroshio path including two branches in ECS; i.e., high salinity gradient region corresponds to KF and TF. The path from south off Taiwan along the east coast of Taiwan is also included. Nevertheless, the gradient is at most 0.1–0.3 psu/100 km, so haline fronts are not discernable under our criterion of >0.5 psu/100 km.

4. Temporal Evolution of Fronts

Figures 11, 12, and 13 show the temporal evolution of the fronts. Fifteen 1° × 1° boxes were used to analyze characteristics of the fronts shown in Fig. 4. The box is labeled "T" ("S") where the thermal (haline) front is dominant. The box is labeled "TS" where both thermal and haline fronts are dominant. The box is labeled "R" where the front does not occur. Figure 11 shows the area-averaged monthly temperature/salinity with its standard deviation (SD-bar) in each box (at 0, 25, 50, and 75 m depths). This standard deviation indicates a temperature/salinity range of the front and is therefore proportional to the frontal intensity. Figure 12 shows the area-averaged monthly frontal intensity (i.e., intensity of temperature/salinity gradient) in each box,

$$\left|\overline{\Delta\psi(t)}\right| = \frac{1}{N}\sum_{i=1}^{N}\sqrt{\left(\frac{\partial\psi(i,t)}{\partial x}\right)^2 + \left(\frac{\partial\psi(i,t)}{\partial y}\right)^2}, \qquad (2)$$

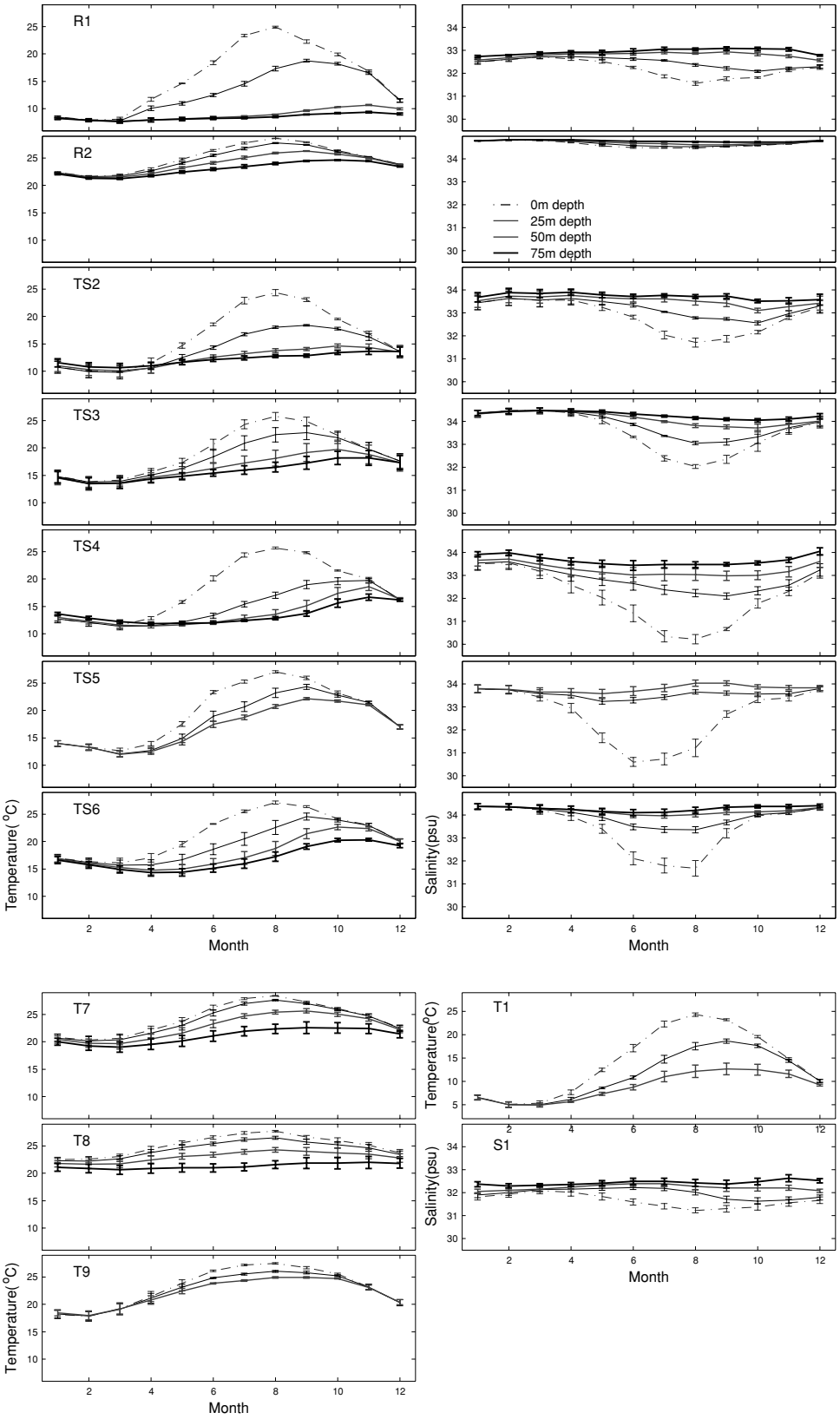

Fig. 11. Monthly variations of area-averaged temperature/salinity (line) with its standard deviation (bar) in each box on the fronts (0, 25, 50, and 75 m depths). Locations and names of the boxes are indicated in Fig. 4.

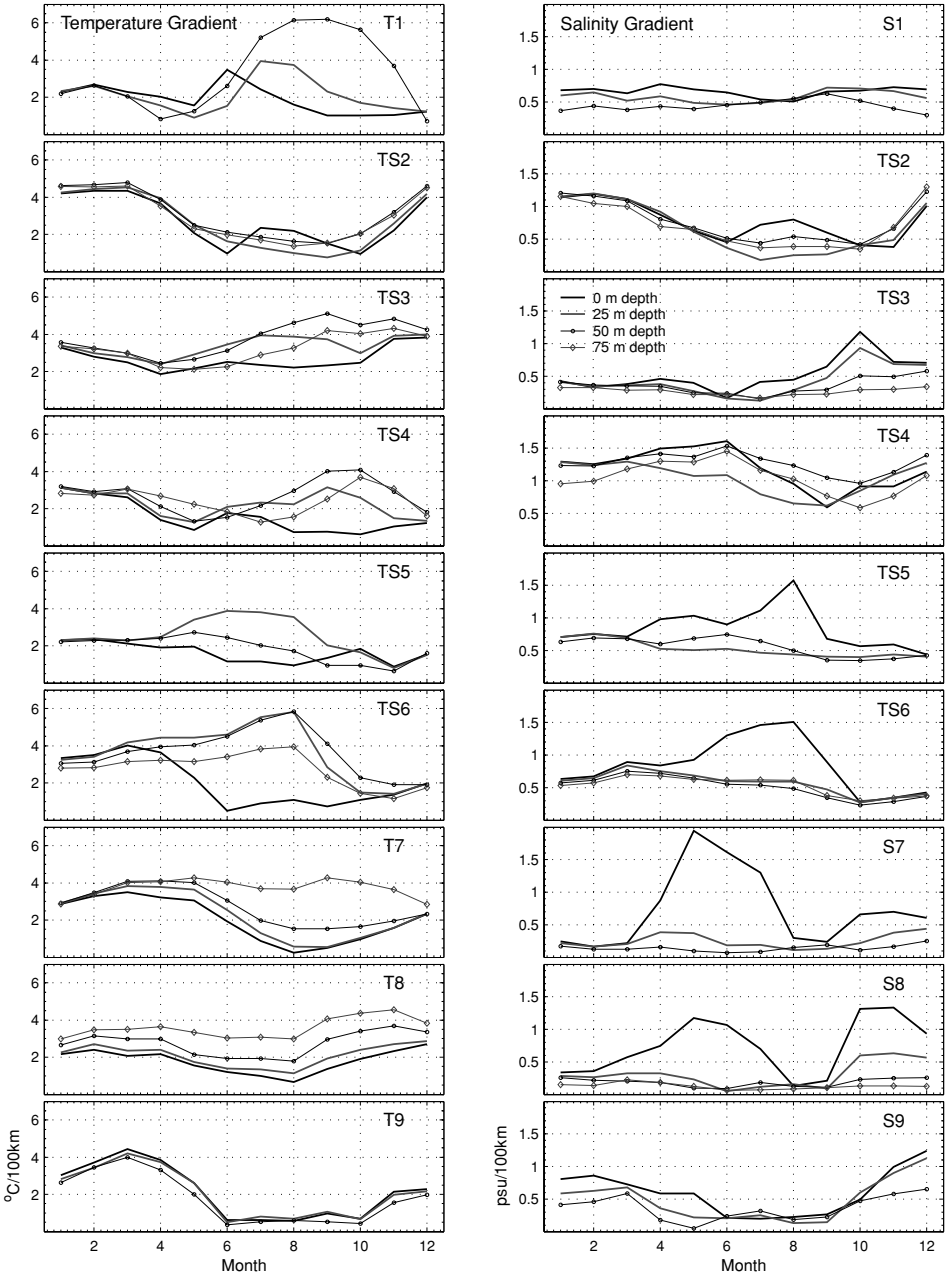

Fig. 12. Monthly variations of frontal intensity at 0, 25, 50, and 75 m depths. Frontal intensity is estimated at area-averaged temperature/salinity gradient in each box on the fronts. Locations and names of the boxes are indicated in Fig. 4.

which was calculated at 0, 25, 50, and 75 m depths. Here, N is the number of data within each box and the other notations are the same as in (1). Figure 13 shows the temporal evolution of (T, S) points (called the T-S evolution curve). The (T, S) values are obtained from profiles at northwestern and southeastern corners of the boxes, except TS4 where the values at the northeastern and southwestern corners are used to represent the direction of CYF.

The evolution curves in the T-S diagrams (Fig. 13) can be classified into two types: clockwise, referred to as Type-1 (see TS6 in Fig. 13), and counterclockwise, referred to as Type-2 (see R1 in Fig. 13). Type-1 (Type-2) is characterized by low salinity in spring (fall) and high salinity in fall (spring). The southeastern corners of TS2 and TS3 and both corners of TS4 generally belong to Type-1, although the salinity increases from January to March due to the Yellow Sea Warm Current and the Tsushima Warm Current. The northwestern corners of TS2

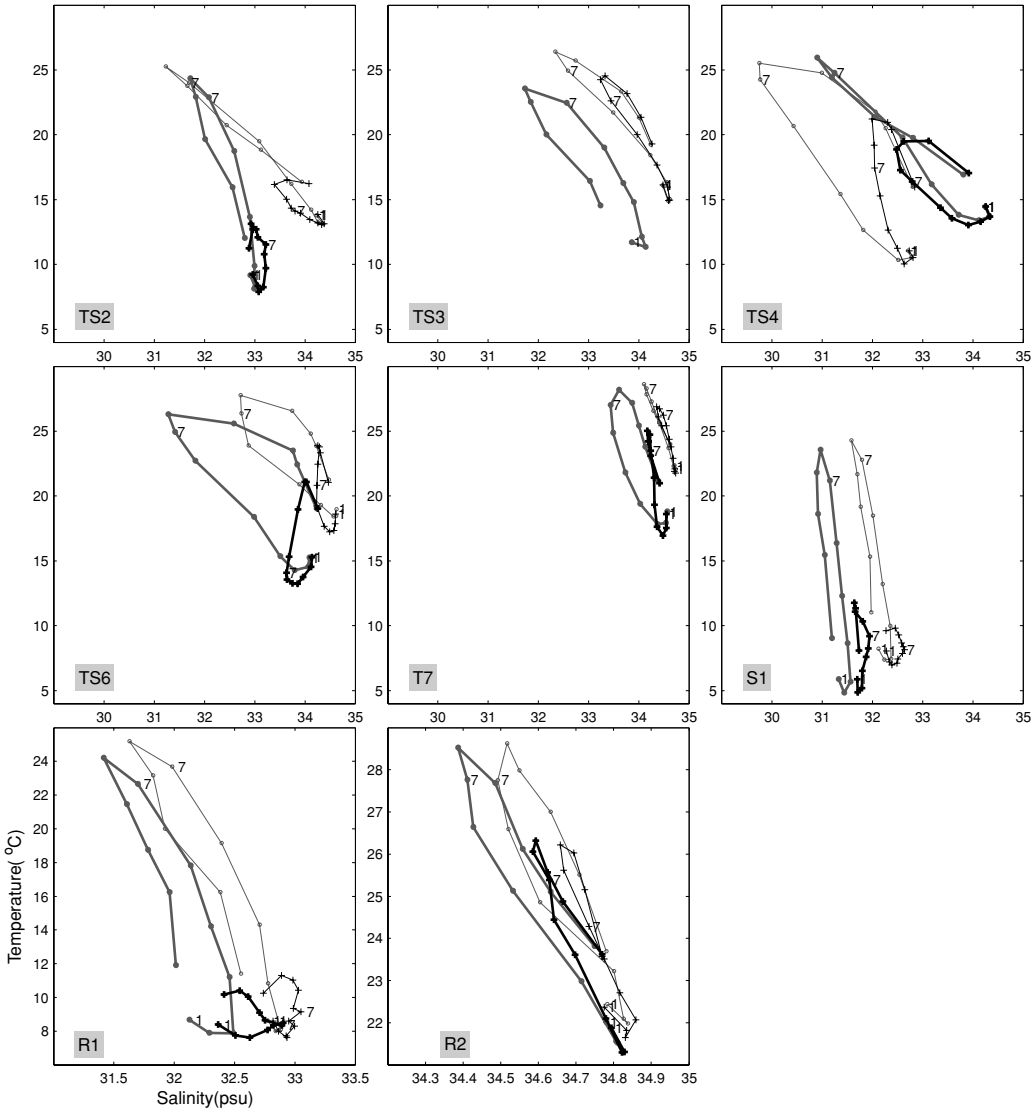

Fig. 13. T-S evolution diagrams of fronts. Gray (black) curve with circles (crosses) is composed of data at 0 m (50 m, 25 m for TS4) depth. Thick (thin) curve indicates data at the northwestern/northeastern (southeastern/southwestern) corner. The label "1" ("7") near the curves represents January (July). No data are available at both 25 m and 50 m depths of the northwestern corner in TS3. Locations and names of the boxes are indicated in Fig. 4.

and TS3 and both corners of S1 and R1 belong to Type-2. According to such a classification, Type-1 (Type-2) represents water mass related to ECS (YS). R2 is close to Type-1 but is characterized by a weak seasonal variation. Especially the salinity variation of R2 is much smaller than those of other boxes. For these reasons, R2 would represent evolution of the Kuroshio water mass.

4.1 Eastern Yellow Sea Front

EYF fully develops with a maximum of 6°C/100 km at 50 m depth from July to November (Fig. 12). It is relatively invariant at the surface and subsurface from December to April in thermal characteristics such as (area-averaged) temperature, temperature range (standard deviation), and frontal intensity (Figs. 11 and 12). Because of the temperature contrast between coastal water (well-mixed by tide) off the west coast of Korea and YSBCW in summer (Choo and Cho, 1984), the thermal characteristics at 50 m depth are also relatively invariant from August to October.

4.2 Western Yellow Sea Front

Salinity in S1 exhibits weak seasonal variation throughout the water column (Figs. 11 and 13). On the

other hand, the salinity difference between the two corners is higher than 0.5 psu throughout the year; the SD-bars at the two corners are nearly equal regardless of depth or month. Temporal variation of frontal intensity is consistent with these features (Fig. 12). WYF is therefore a year-round with steady frontal intensity throughout the water column.

4.3 Cheju-Yangtze Front

4.3.1 Northern tongue of Cheju-Yangtze Front

TS2 has the same density range of seasonal variation as TS3 from November to May (not shown), but is 3°C cooler and 0.5 psu fresher than TS3. This density variation may imply that the water mass of TS2 is dynamically related to that of TS3 and that the northern tongue of CYF is connected to CTF. However, from June to October the water mass of TS3 resembles that of TS6.

The northern tongue of CYF is maintained by two water masses, because TS2 is composed of two different types of evolution curves, Type-1 at southeastern corner and Type-2 at northwestern corner (Fig. 13). The (T, S) curves at different depths evolve in the same direction (i.e., the same type), which shows that the northern tongue varies vertically in phase through the water column. This vertical in-phase variation is also shown in the temporal variation of frontal intensity of TS2 with strong (weak) frontal intensity in winter (summer) (Fig. 12). Moreover, the frontal intensity of the thermal northern tongue evolves in-phase with that of the haline tongue. The thermal (haline) northern tongue is controlled by the water mass evolution at the northwestern (southeastern) corner, because temperature (salinity) variation is more dominant at the northwestern (southeastern) corner than at southeastern (northwestern) corner.

4.3.2 Southern tongue of Cheju-Yangtze Front

Temperature and salinity gradients in TS4 and TS5 are strong at the subsurface throughout the year, despite a seasonal variability of intensity; i.e., the southern tongue of thermal/haline CYF is persistent at subsurface (Fig. 12). The haline tongue is strongest among subsurface haline fronts. At 25 m depth, the T-S evolution curve at the southwestern corner of TS4 (relatively shallow bottom topography of the Yangtze Bank) shows strong seasonal variation in temperature (Fig.13). In contrast, the T-S evolution curve at the northeastern corner of TS4 shows stronger seasonal variation in salinity. Therefore, at 25 m depth the seasonal temperature (salinity) variation at the southwestern (northeastern) corner is responsible for the variability of the southern tongue of thermal (haline) CYF.

4.4 Tsushima Front

The temperature gradient of TS6 shows the strong TF with a maximum intensity of 6°C/100 km at the subsurface from spring to summer (Fig. 12). The cold water (<15°C) over the Yangtze Bank, shown at 50 m depth of the northwestern corner from January to August, contributes to such a strong frontal intensity (Fig. 13). Although salinity variation in the T-S evolution curves at the southeastern corner of TS6 is large due to mixing with the fresh ECS shelf water, the T-S evolution curves of TS6 resemble those at the northwestern corner of T7. This similarity implies relationship between TF and KF.

4.5 Yangtze Ring Front

From March to July the surface salinity in TS4 decreases rapidly with large SD-bar, indicating a continuous supply of the low salinity water (Fig. 11). Consistently, TS4 has a maximum salinity gradient of 1.3–1.6 psu/100 km from spring to summer (Fig. 12), leading to an evident northern arc of YRF. On the other hand, the salinity SD-bar of TS5 and TS6 at the surface is rather large as the salinity reaches a minimum from June to August, but not during the rapid salinity decrease from March to June (Fig. 11). Such an SD-bar variation shows a distinguishable southern arc of YRF in summer and a strong surface salinity gradient in TS5 and TS6 (Fig. 12).

4.6 Cheju-Tsushima Front

CTF exists throughout the depth all year round (Fig. 12). TS3 has two different types of evolution curves: Type-1 at the southeastern corner and Type-2 at the northwestern corner. At the surface the two curves maintain an equal distance from January to July and then evolve in the opposite direction (Fig. 13). As a result the frontal intensity (4–5°C/100 km) becomes stronger after August (Fig. 12). From September to October TS3 has low salinity at the surface and 25 m depth, which is comparable with that in TS6 (Fig. 11). At the northwestern corner, the salinity decreases significantly from July to August and remains low (<32.0 psu) by October due to the migration of the Yangtze River Diluted Water toward the Korean Strait (Fig. 13). Accordingly the salinity gradient of CTF increases from July to October (Fig. 12). This feature is also detected at 25 m depth (Fig. 12).

4.7 Kuroshio Front and minor fronts near Taiwan

At 75 m depth the temperature gradient of T7 on KF persists all year round with a constant intensity of 4°C/100 km, whereas at other depths it varies with season (Fig. 12). The T-S evolution curves at the southeastern corner of T7 resemble those of R2 (Fig. 13). The temperature gradient of T8 (northeast off Taiwan) is strong all year round and varies almost in phase at all depths, with weaker intensity at shallower depth (Fig. 12). Its seasonal variation is similar to that of T7 at 75 m depth. These features show year-round Kuroshio intrusion into the ECS shelf (Chuang and Liang, 1994; Tang *et al.*, 2000). The tem-

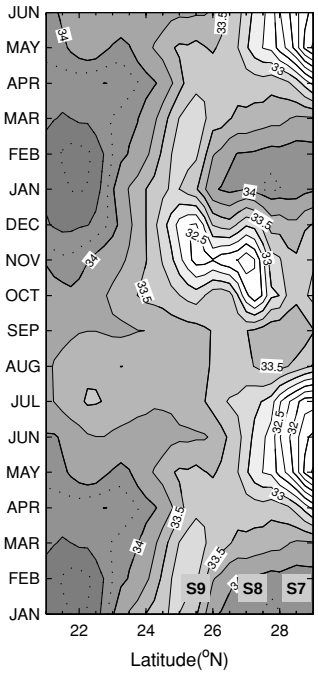

Fig. 14. Time-distance plots of sea surface salinity along a straight line labeled "3" in Fig. 4. Sea surface salinity from January to June is plotted repeatedly after December.

perature gradient of T9 in the Taiwan Strait shows prominent seasonal variation with in-phase variation throughout the depth: a strong gradient from November to May and a weak gradient from June to October (Fig. 12). Strengthening of the frontal intensity in winter is caused by the winter blocking, as described in Subsection 3.2, whereas weakening in summer (reduction of SD-bar) is caused by the advance of the Taiwan Warm Current (Fig. 11).

4.8 Chinese Coastal Front

From January to February no low salinity plume is detected in S7 and S8, whereas a low salinity plume (33.25 psu) with high gradient is detected in S9 (Figs. 8 and 14). This low salinity plume moves northward along the Zhejiang-Fujian coast during the winter to summer monsoon transition (Fig. 14). This phenomenon is also detected from CMA (Fig. 2). Accordingly, the salinity gradient in S9 (S7 and S8) decreases (increase) gradually from March to April (Fig. 12).

In May this low salinity patch finally merges into the tail of the Yangtze River plume that occurs in April, and the tail of the plume extends southward to 27°N along the Zhejiang-Fujian coast (Figs. 8 and 14). As a result, the salinity gradient of S7 and S8 reaches a maximum with an intensity of 1–2 psu/100 km (Fig. 12). This tail persists from May to July but disappears or migrates seaward in August owing to the intensification of the Taiwan Warm Current and the prevailing southwesterly summer monsoon (Figs. 8 and 14). This feature is maintained in September and is consistent with a very weak salinity gradient of S7 and S8 from August to September (Fig. 12).

At the onset of the northeasterly winter monsoon in October, the Yangtze River plume hugs the Zhejiang-Fujian coast in a narrow band. A new low salinity plume (~32.25 psu) is formed at 121°E and 27.5°N in October (Figs. 8 and 14), which might be shed from the Yangtze River plume and/or the river along the Zhejiang-Fujian coast. This new low salinity plume travels southward during the prevailing northeasterly winter monsoon. Consistently, the salinity gradient of S7 and S8 increases to the second peak from October to November and then decreases, while that of S9 increases during that time. The salinity gradient of S9 maintains an intensity of >0.6 psu/100 km until next spring. The low salinity plume does not travel further south of 23°N and is expected to travel northward again next spring (Fig. 14).

5. Lag-Correlation of Temperature/Salinity on Fronts

To examine the linkage among the fronts in terms of seasonal variations of water mass on the fronts, lag-correlation coefficients (LCCs) are calculated among temperature/salinity time series at the northwestern (n-)/southeastern (s-) corners of all the boxes in Fig. 4 except for TS4 where the northeastern and southwestern corners are used. Two reference time-series are chosen to represent the YS water mass (n-corner of R1) and the Kuroshio water mass (s-corner of R2). LCC of temperature (salinity), referred to as LCC-T (LCC-S), is computed with these reference time-series.

At the surface all LCC-Ts are nearly the same among any pairs, because the sea surface temperature is strongly influenced by the regional heat balance (not shown). At 50 m depth the s-corner of R2 varies almost simultaneously with the s-corner of TS3 (s-corner of T7 leads s-corner of R2 a little); that is, the seaward side of the corresponding fronts is affected by the water originating from the Kuroshio water (Fig. 15(b)). The s-corner of R2 leads s-corners of R1, S1, and TS2 with 1–2 months. In other words, the s-corner of R2 (R1) shows a maximum temperature in September (October to November). This lag is due to slow heat transfer through the strong thermocline walls surrounding YSBCW. The s-corner of TS6 lags the s-corner of R2 by 0–1 month than the s-corner of TS3, though TS6 is closer to R2 than TS3. The n-corner of R1 varies almost simultaneously with the n-corner of TS6 and leads the n-corner of TS4 a little (Fig. 15(a)). This lag-correlation of R1 to TS4 and TS6 suggests that the southern tongue of CYF and TF are influenced by cold water present to their northern (shoreward) side. Overall,

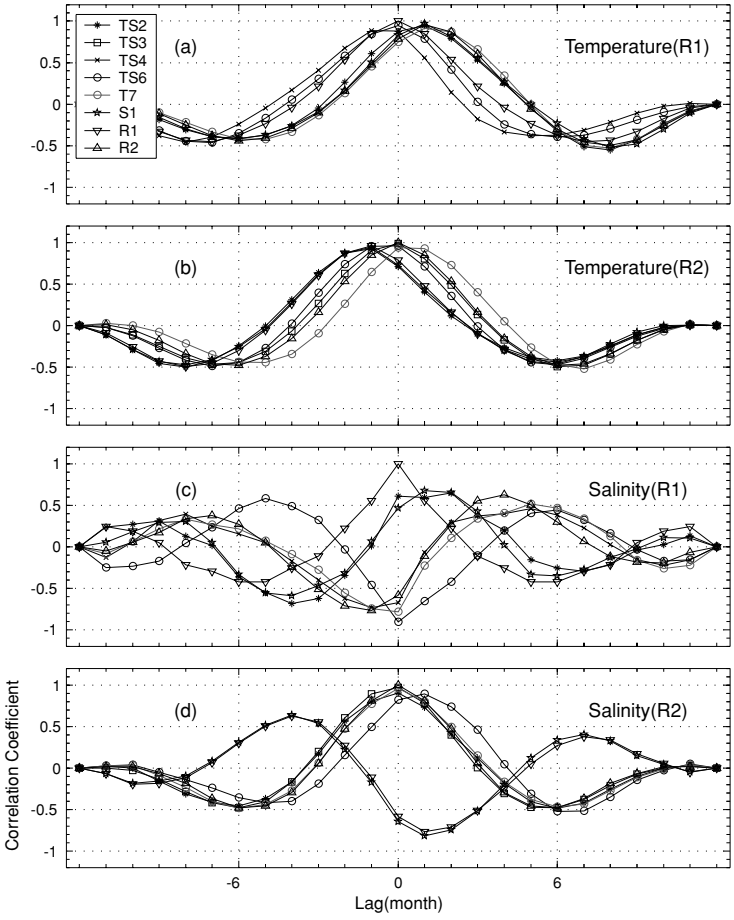

Fig. 15. Lag-correlation coefficients (LCC) of each box with reference box: (a) LCC-T with reference R1, (b) LCC-T with reference R2, (c) LCC-S with reference R1, and (d) LCC-S with reference R2. Negative lag indicates the lead of the reference time-series.

a maximum lag among the boxes does not exceed two months.

LCC-Ss at the surface are lagged, unlike LCC-Ts. The n-corner of R1 lags the n-corners of TS4, R2, TS6, and T7 by 1 month and varies almost simultaneously with the n-corners of TS2, TS3, and S1 (not shown), which is consistent with the net fresh water flux reaching a maximum in July (June) in YS (ECS) (Chu *et al*., 2005). At 50 m depth, the s-corner of R2 varies almost simultaneously with the s-corners of TS3, T7, and TS2; therefore, the s-corners TS3, T7, and TS2 is influenced by the water originating from the Kuroshio water (Fig. 15(d)). Moreover, the s-corner of R2 shows negative correlation with the s-corners of R1 and S1 at –1 month lag. In the regions of R1 and S1 salinity decreases in winter due to the wintertime strong vertical mixing and increases from spring to summer due to the weak mixing and/or advection. Therefore, minimum salinity occurs in winter and maximum salinity occurs in summer. Likewise, the n-corner of R1 shows negative correlation with the n-corners of the boxes over ECS (Fig. 15(c)).

6. Conclusions

The Yellow/East China Sea thermal and haline fronts detected from GDEM agree quite well with those from in-situ and satellite observations in terms of locations and time (month). Their seasonality at the surface and subsurface is compared in terms of spatial features, frontal intensity, and temporal evolutions of temperature and salinity on the front (Table 1).

The density-compensated Cheju-Yangtze Thermal/Haline Front has a two-tongued shape. Its northern tongue is characterized by warm saline water intrusion and the southern thermal tongue is mainly maintained by the coastal water off the Shandong peninsula-Jiangsu coast and the Yellow Sea Bottom Cold Water. The southern

Table 1. Frontal characteristics in the Yellow and the East China Seas.

Front	Seasonality
Thermal front	
Eastern Yellow Sea Front (EYF)	Relatively invariant throughout the depth from December to April and fully developed at 50 m depth from July to November
Cheju-Yangtze Thermal Front (thermal CYF)	
northern tongue	Strong frontal intensity throughout the depth from December to April
southern tongue	Persistent at subsurface despite seasonal migration
	Turning its direction from southeastward to southward and then joining KF at its southern margin from spring to summer
Tsushima Front (TF)	Strong at subsurface from March to September
	A northern branch of the Kuroshio Front, usually joining the eastern part of the southern tongue of CYF in summer
Cheju-Tsushima Front (CTF)	Year-round throughout the depth and enhanced from July to December
Kuroshio Front (KF)	Evident at depths shallower than 75 m from November to May
	Nearly motionlessly at depths deeper than 100 m all year round despite slight seasonal-change of frontal intensity at ~100 m depth
Haline front	
Western Yellow Sea Haline (WYF)	Year-round with steady frontal intensity throughout the depth
Cheju-Yangtze Haline Front (haline CYF)	
northern tongue	In-phase evolution between its thermal and haline frontal intensities
southern tongue	Nearly motionless and most evident at subsurface all year round
Yangtze Ring Front (YRF)	Manifest from spring to summer for its northern arc and full development of its southern arc in summer
Chinese Coastal Front (CCF)	Seasonal shift of the region with maximum frontal intensity: near the Taiwan Strait from November to March, moving northward along the Zhejiang-Fujian coast in April, staying near the Zhejiang coast from May to July, weakening from August to September, and then moving southward afterward

haline tongue is distinguished at the subsurface throughout the year owing to the Kuroshio water intrusion in the bottom friction layer at the Yangtze Relict River valley. The Yangtze Haline Ring Front is strongest in the Yellow/East China Sea, which is restricted from the surface to 15 m depth. The plumes shed from the Yangtze River and/or neighboring rivers generate the Chinese Coastal Haline Front. The monsoon and the Taiwan Warm Current cause the variations of these surface haline fronts.

The water masses of the northern tongue of the Cheju-Yangtze Front and the Cheju-Tsushima Front have comparable seasonal variability. The Tsushima Front resembles the Kuroshio Front in the T-S evolution curve. The water mass northeast of Taiwan also resembles that of the Kuroshio Front. These relations of water masses among the fronts imply that the generation and evolution of the fronts are closely associated with the YES circulation.

The northern tongue of Cheju-Yangtze Front and the Cheju-Tsushima Front are composed of the two different types of T-S evolution curve: the Yellow Sea water mass type and the East China Sea water mass type. Accordingly, mixing around these two fronts is vigorous in both temperature and salinity fields. At both surface and subsurface the frontal intensity of the northern tongue of Cheju-Yangtze Thermal (Haline) Front is determined mainly by the temperature (salinity) variation on its shoreward (seaward) side. The southern tongue is evident only at the subsurface. At 50 m depth the water on the shoreward side is related to the Yellow Sea water mass type, which reaches a maximum temperature 1–2 months later than the East China Sea/Kuroshio water mass. However, the sea surface salinity of the East China Sea/Kuroshio water mass type varies one month ahead of that of the Yellow Sea water mass type, whereas the subsurface (50 m) one is out-of-phase. Local factors, such as the wintertime intense vertical mixing and the summertime strong thermocline above the Yellow Sea Bottom Cold Water, cause different subsurface (50 m) temperature and salinity evolutions in the Yellow Sea and in the East China Sea.

The cold water over the Yangtze Bank intruded from the Yellow Sea trough to the south, which is provided by the southward coastal currents along the Shandong peninsula-Jiangsu coast, influences the seasonal variability of the fronts. It generates the southern tongue of the Cheju-Yangtze Front and shifts this southern tongue toward the Kuroshio Front in spring. It shifts this southern tongue toward the Tsushima Front in summer and then intensifies the Tsushima Front. How this cold water regulates the circulations in the southern Yellow Sea and the northern East China Sea needs to be explored in further studies.

Acknowledgements

This work was supported by the Office of Naval Research, Naval Oceanographic Office, and the Naval Postgraduate School.

Nomenclature List

AXBT	airborne expendable bathythermograph
CCF	Chinese Coastal Front
CMA	China Marine Atlas
CTF	Cheju-Tsushima Front
CYF	Cheju-Yangtze Front
ECS	East China Sea
EYF	eastern Yellow Sea Front
GDEM	Generalized Digital Environmental Model
KF	Kuroshio Front
LCC	Lag-correlation coefficient
MOODS	Master Oceanographic Observation Data Set
TF	Tsushima Front
WYF	western Yellow Sea Front
YES	Yellow/East China Seas
YRF	Yangtze Ring Front
YS	Yellow Sea
YSBCW	Yellow Sea Bottom Cold Water

References

Beardsley, R. C., R. Limeburner, L. Kentang, H. Dunxin, G. A. Cannon and D. J. Pashinski (1983): Structure of the Changjiang River plume in the East China Sea during June 1980. p. 265–284. In *Proceedings of International Symposium on Sedimentation on the Continental Shelf, with Special Reference to the East China Sea*, Vol. 1, China Ocean Press, Beijing.

Chang, P. and A. Isobe (2003): A numerical study on the Changjiang diluted water in the Yellow and East China Seas. *J. Geophys. Res.*, **108**(C9), 3299, doi:10.1029/2002JC001749.

Chen, C., R. C. Beardsley, R. Limeburner and K. Kim (1994): Comparison of winter and summer hydrographic observations in the Yellow and East, China Sea and adjacent Kuroshio during 1986. *Cont. Shelf Res.*, **14**, 909–929.

China Ocean Press (1992): *Marine Atlas of Bohai Sea, Yellow Sea, and East China Sea, Hydrology*. China Ocean Press, Beijing, 524 pp.

Choo, H. S. and K. D. Cho (1984): The structure of tidal front in the eastern Yellow Sea in the summer of 1982. *Bulletin of Korean Fisheries Society*, **17**(2), 83–91 (in Korean with English abstract).

Chu, P. C. and G. Wang (2003): Seasonal variability of thermohaline front in the central South China Sea. *J. Oceanogr.*, **59**(2), 65–78.

Chu, P. C., C. R. Fralick, S. D. Haeger and M. J. Carron (1997a): A parametric model for Yellow Sea thermal variability. *J. Geophys. Res.*, **102**(C5), 10499–10508.

Chu, P. C., S. K. Wells, S. D. Haeger, C. Szczechowski and M. Carron (1997b): Temporal and spatial scales of the Yellow Sea thermal variability. *J. Geophys. Res.*, **102**(C3), 5655–5668.

Chu, P. C., Y. C. Chen and A. Kuninaka (2005): Seasonal variability of the East China/Yellow Sea surface buoyancy flux and thermohaline structure. *Advances in Atmospheric Sciences*, **22**, 1–20.

Chuang, W. S. and W. D. Liang (1994): Seasonal variation of the Kuroshio water across the continental shelf northeast of Taiwan. *J. Oceanogr.*, **50**, 531–542.

Furey, H. and A. Bower (2005): The synoptic Temperature Structure of the East China and southeastern Japan/East Seas. *Deep-Sea Res. II*, **52**, 1421–1442.

Gao, Y., R. Arimoto, R. A. Duce, D. S. Lee and M. Zhou (1992): Input of atmospheric spring of a low-dust year. *J. Geophys. Res.*, **97**(D4), 3767–3777.

Guan, B.-X. (1994): Patterns and structures of the currents in Bohai, Huanghai and East China Seas. p. 17–26. In *Oceanology of China Seas*, Vol. 1, ed. by D. Zhou, Y.-B. Liang and C. K. Tseng, Academic Publishers.

Hao, W., J. Su, R. Wan, L. Wang and Y. Lin (2003): Tidal front and the convergence of anchovy (*Engraulis japonicus*) eggs in the Yellow Sea. *Fish. Oceanogr.*, **12**(4/5), 434–442.

Hickox, R., I. M. Belkin, P. Cornillon and Z. Shan (2000): Climatology and seasonal variability of ocean fronts in the East China, Yellow and Bohai Seas from satellite SST data. *Geophys. Res. Lett.*, **27**(18), 2945–2948.

Hsueh, Y. (1988): Recent current observations in the eastern Yellow Sea. *J. Geophys. Res.*, **93**(C6), 6875–6884.

Hsueh, Y. (2000): The Kuroshio in the East China Sea. *J. Mar. Sys.*, **24**, 131–139.

Huh, O. K. (1982): Spring-season flow of the Tsushima Current and its separation from the Kuroshio: satellite evidence. *J. Geophys. Res.*, **87**(C12), 9687–9693.

Ichikawa, H. and R. C. Beardsley (2002): Review: The Current System in the Yellow and East China Seas. *J. Oceanogr.*, **58**(1), 77–92.

Isobe, A. (1999): The Taiwan-Tsushima Warm Current system: its path and the transformation of the water mass in the East China Sea. *J. Oceanogr.*, **55**(2), 185–195.

Ivanov, A. Y., W. Alpers, K. T. Litovchenko, M. He, Q. Feng, M. Fang and X. Yan (2004): Atmospheric front over the East China Sea studied by multisensor satellite and in situ data. *J. Geophys. Res.*, **109**, C12001, doi:10.1029/2004JC002432.

Jacobs, G. A, W. J. Teague, S. K. Reindlinger and R. H. Preller (1998): Sea surface height variation in the Yellow and East China Seas: 2. SSH variability in the weekly and semiweekly bands. *J. Geophys. Res.*, **103**(C9), 18479–18496.

Jacobs, G. A., H. B. Hur and S. K. Riedlinger (2000): Yellow and East China Seas response to winds and currents. *J. Geophys. Res.*, **105**(C9), 21947–21968.

Jacobs, G. A., H. T. Perkins, W. J. Teague and P. J. Horgan (2001): Summer transport through the Tsushima-Korea Strait. *J. Geophys. Res.*, **106**(C4), 6917–6929.

Jan, S., J. Wang, C.-S. Chern and S.-Y. Chao (2002): Seasonal variation of the circulation in the Taiwan Strait. *J. Mar. Sys.*, **35**(3/4), 249–268.

Lee, H. J. and S. Y. Chao (2003): A climatological description of circulation in and around the East China Sea. *Deep-Sea Res. II*, **50**, 1065–1084.

Lee, H. J., S.-Y. Chan and K.-K. Liu (2004): Effects of reduced Yangtze River discharge on the circulation of surrounding seas. *Terr. Atmos. Ocean. Sci.*, **15**(2), 111–132.

Lee, J.-H., H.-J. Lie and C.-H. Cho (2003): The structure of ocean fronts in the East China Sea. p. 2-10-1~2. In *Proceedings of the 12th PAMS/JECSS Workshop*, Hangzhou, China.

Lie, H.-J. (1989): Tidal fronts in the southeastern Hwanghae (Yellow Sea). *Cont. Shelf Res.*, **9**(6), 527–546.

Lie, H.-J., C.-H. Cho, J.-H. Lee, S. Lee and Y. Tang (2000): Seasonal variation of the Cheju Warm Current in the Northern East China Sea. *J. Oceanogr.*, **56**(2), 197–211.

Lie, H.-J., C.-H. Cho, J.-H. Lee, S. Lee, Y. Tang and E. Zou (2001): Does the Yellow Sea Warm Current really exist as a persistent mean flow? *J. Geophys. Res.*, **106**(C10), 22199–22210.

Lie, H.-J., C.-H. Cho, J.-H. Lee and S. Lee (2003): Structure and eastward extension of the Changjiang River plume in the East China Sea. *J. Geophys. Res.*, **108**(C3), 3077, doi:10.1029/2001JC001194.

Liu, G. M., S. Sun, H. Wang, Y. Zhang, B. Yang and P. Ji (2003): Abundance of Calanus sinicus across the tidal front in the Yellow Sea, China. *Fish. Oceanogr.*, **12**(4/5), 291–298.

Naimie, C. E., C. A. Blain and D. R. Lynch (2001): Seasonal mean circulation in the Yellow Sea—a model-generated climatology. *Cont. Shelf Res.*, **21**, 667–695.

Ning, X., Z. Liu, Y. Cai, M. Fang and F. Chai (1998): Physicobiological oceanographic remote sensing of the East China Sea: Satellite and in situ observations. *J. Geophys. Res.*, **103**(C10), 21623–21635.

Oka, E. and M. Kawabe (1998): Characteristics of variations of water properties and density structure around the Kuroshio in the East China Sea. *J. Oceanogr.*, **54**, 605–617.

Park, K.-A., J. Y. Chung and K. Kim (2004): Sea surface temperature fronts in the East (Japan) Sea and temporal variations. *Geophys. Res. Lett.*, **31**, L07304, doi:10.1029/2004GL019424.

Perkins, H., W. Teague, G. Jacobs, K.-I. Chang and M.-S. Suk (2000): Currents in Korea-Tsushima Strait during summer 1999. *Geophys. Res. Lett.*, **27**, 3033–3036.

Qui, B., T. Toda and N. Imasato (1990): On Kuroshio front fluctuations in the East China Sea using satellite and in situ observational data. *J. Geophys. Res.*, **95**(C10), 18191–18204.

Riedlinger, S. K. and G. A. Jacobs (2000): Study of the dynamics of wind-driven transports into the Yellow Sea during winter. *J. Geophys. Res.*, **105**(C12), 28695–28708.

Seung, Y. H. and S. I. Shin (1996): A simple model of the formation of thermohaline front in the southeastern YS in winter. *J. Korean Soc. Oceanogr.*, **31**(1), 23–31.

Son, Y.-T., S.-H. Lee, J. C. Lee and J.-C. Kim (2003): Water masses and frontal structures in winter in the northern East China Sea. *J. Korean Soc. Oceanogr. (The Sea)*, **8**(3), 327–339 (in Korean with English abstract).

Tang, T. Y., J. H. Tai and Y. J. Yang (2000): The flow pattern north of Taiwan and the migration of the Kuroshio. *Cont. Shelf Res.*, **20**(4/5), 349–371.

Teague, W. J. and G. A. Jacobs (2000): Current observations on the development of the Yellow Sea Warm Current. *J. Geophys. Res.*, **105**(C2), 3401–3411.

Tseung, C., C. Lin, S. Chen and C. Shyu (2000): Temporal and spatial variations of sea surface temperature in the East China Sea. *Cont. Shelf Res*., **20**(4/5), 373–387.

Xie, S.-P., J. Hafner, Y. Tanimoto, W. T. Liu, H. Tokinaga and H. Xu (2002): Bathymetric effect on the winter sea surface temperature and climate of the Yellow and East China Seas. *Geophys. Res. Lett.*, **29**, 2228, doi:10.1029/2002GL015884.

Zhao, B. (1987): The continental shelf fronts induced by tidal mixing in the Huanghai Sea. *Journal of Oceanography of Huanghai and Bohai Seas*, **5**(2), 16–23 (in Chinese with English abstract).